VERSITA

OPTO-ELECTRONICS REVIEW **20**(2), 174–186

DOI: 10.2478/s11772-012-0026-x

Multistage morphological segmentation of bright-field and fluorescent microscopy images

A. KORZYŃSKA*[1] and M. IWANOWSKI[2]

[1]Nałęcz Institute of Biocybernetics and Biomedical Engineering PAS, 4 Ks. Trojdena Str., 02–109 Warsaw, Poland
[2]Institute of Control and Industrial Electronics, Warsaw University of Technology, 75 Koszykowa Str., 00–662 Warsaw, Poland

This paper describes the multistage morphological segmentation method (MSMA) for microscopic cell images. The proposed method enables us to study the cell behaviour by using a sequence of two types of microscopic images: bright field images and/or fluorescent images. The proposed method is based on two types of information: the cell texture coming from the bright field images and intensity of light emission, done by fluorescent markers. The method is dedicated to the image sequences segmentation and it is based on mathematical morphology methods supported by other image processing techniques. The method allows for detecting cells in image independently from a degree of their flattening and from presenting structures which produce the texture. It makes use of some synergic information from the fluorescent light emission image as the support information. The MSMA method has been applied to images acquired during the experiments on neural stem cells as well as to artificial images. In order to validate the method, two types of errors have been considered: the error of cell area detection and the error of cell position using artificial images as the "gold standard".

Keywords: image segmentation, microscopic image of living cells, bright field images, fluorescent images, epi-fluorescent images, texture analysis, watershed.

1. Introduction

1.1. Subject of paper

In this paper, a novel method of microscopic images segmentation of living cells is proposed. This method called multistage morphological segmentation method (MSMA) allows for extracting the area covered by the cell or cells' clone from the pair of images captured in order to document the cells' behaviour as a sequence of images. The aim of this investigation is to develop a method of segmentation dedicated to the microscopic images of stem cells growing in culture in two cases – when cells' population under observation is with and without fluorescent protein inside or on the surface of cell's membrane. The MSMA method is developed for images captured using time-laps microscopy. The microscope output images are captured using either exclusively bright field microscopic (BF images) technique or BF technique supported by fluorescent markers (EF images). The images are captured for each view field one by one with a hardware delay, which is significantly shorter than a time increment used for an observation of the behaviour. The second type of observation is performed on cells stained with the fluorescent markers or transfected by the fluorescent proteins.

The method is based on mathematical morphology approach supported by other image processing techniques, such as thresholding and texture analysis. The method consists of two stages: the coarse segmentation stage followed by the fine segmentation stage. The coarse segmentation stage aims at finding a map pointing at particular cells. At this stage only the presence of cells within the images is detected. Two tracks of the coarse segmentation are proposed, the first is based on the BF-images, while the second – on the EF-ones. The results of both are complementary and are combined based on the shape of particular cells. Finally, the combined result of coarse segmentation is refined in the second stage of the method called fine segmentation. This stage is based on morphological watershed transform and it results in the precise outline of cells.

The paper consists of 4 sections. Section 1 is the introduction. Section 2 presents the proposed method. Section 3 shows the results of proposed method. The last Sect. 4 contains the discussion and conclusion.

1.2. Previous works

Quantification of cells' behaviour from sequences of microscopic images is important for many studies, i.e., for regenerative medicine [1–6], hematology [7–11], oncology [12, 13], and for biological research on cell's movement and motility of cells [14–17].

*e-mail: anna.korzynska@ibib.waw.pl

In order to analyse cells' behaviour, the images captured in sequences should be segmented into objects on each frame separately and then the objects should be matched from one frame to the other. Cells' behaviour is described by changes in time of such their features as cells' area, shape, intensity distribution and others. To achieve sufficiently precise description of cells' behaviour, as the first step of analysis, the image segmentation should be performed with relevant precision adjusted to the aim of investigation [18]. Well known and simple segmentation methods [19–23], such as various types of thresholdings, gradient and edge examination and clustering are effective for ideal images. An ideal image means in this case an image which is acquired by having the possibility of adjusting parameters of acquisition. These parameters such as contrast, level of details in image/objects are thus optimal for a particular single image. Such image shows one or several well separated and relatively uniform objects. The ideal images are used in robotics, security, biometry and in some medical diagnostics. In the latter, they are applied to recognize, e.g., cancerous cells in a fixed microscopic sample from cytological smears [24–26] or tissue sections [27–30]. During the observations of living cells, where the cells' population behaviour is monitored in biological experiments or for medical diagnostics or prognosis, an operator cannot interfere in the process of image capturing. In the process of the image sequence acquisition, controlled by computer software, the most of acquisition parameters are chosen only once initializing the process, independently of external conditions' variations such as decrease in the fluorescent signal and increase in density of the cell in an image plane. Consequently, the acquired images and the cells in the images slightly differ from one frame to another and from one sequence to another.

Fully automatic methodology of the microscopic image segmentation described in literature [1,11] is adjusted to the specific and relatively homogeneous in appearance cells' population and to the images captured by using a specific type of microscopic techniques. For example, methodology presented in Ref. 1 was developed for mitotic cell detection in the HeLa cells in a culture observed in phase contrast microscopic techniques. This type of cells is characterized by a circular shape, small size variations and homogenous pixels intensity within the region of cells' body. The methodology of segmentation proposed in Ref. 2 for microscopic fluorescence images is easy but precise enough only when the cells are homogenous in lighting both across each cell and from one cell to another. It the both above methods, it is not explicitly assumed that the cells are surrounded by a background and do not touch one another. In such a case, when a segmented object consists of multiple cells, the question how to separate the cells touching each other remains open.

The semi-automatic methodology of the image segmentation with operator's intervention is mainly presented in literature about microscopic images segmentation [24]. This idea is also exploited in the presented investigations.

1.3. Assumptions

The microscopic images of cells' samples can be acquired by using various techniques of microscopy. Among them there are: bright-field (BF) technique of transmitted light microscopy, phase contrast technique – typically used in cell observations and the other interference contrast images (e. g., Nomarski technique) or dark field techniques. Other microscopic techniques frequently used for living cells' observations are based on the phenomenon of fluorescence. One of them is epi-fluorescent technique (EF) which shows light emission coming from the fluorescent protein attached to the cells' surface or organelles or just secreted to the cytoplasm.

Cells observation can be done both in non-coherent and coherent light. The last one allows to achieve a very thin deep of field and to observe a particular slice of the cell while the first one integrates the signal across the cell.

All microscopic techniques produce images of different characteristics with various objects' details visible. The BF images show details of the cell's morphology along with a stream of light coming through the cell body and the edges while the confocal images show details of a thin slice of the cell. The phase contrast microscopy covers the borders of cells with a strong halo, so the pods formed by the cells are hidden. The fluorescent images of cells show objects as a mosaic of the various intensity bright spots on the dark background.

Each type of living cells' images has various advantages and disadvantages from the point of view of information required for the image processing and the analysis methods. Unfortunately, neither type of microscopic images shows enough details and features which may be required to define of the accurate and precise algorithm for the single cell segmentation in all cases. In such a case, it must be decided whether to collect the information about the cells from the BF images only or from the BF and EF images, simultaneously. In the second case, both images are acquired one by one with the smallest possible hardware time delay t_{delay} which is much more smaller than the chosen behaviour observations' time increment Δt and which is negligibly compared with the time scale of the observed phenomenon such as the cells' crawling movement, the cells' proliferation, necrosis or apoptosis.

The method proposed in this paper makes use of the BF images either supported by the EF images or not. It constructs a map of the objects B_i in the particular time t based on the following observations and assumptions:

- in most cases, information about cells contained in each single image is not sufficient to find each cell's location. Due to this fact, the information coming from two cell-imaging methods (BF and EF) is used. Both image sources provide us with the different aspects of cell presence in a certain place (see Figs. 1 and 2). It must be, however, taken into consideration that the EF-image is absent or its quality is poor (the contrast between cells and the background is too low). So, it is assumed, that

the method should be effective even in the case of problems with EF-image,

- while cells' population under observation is biologically homogeneous, simultaneously it is non-homogenous in the terms of cells' morphology/appearance (see Figs. 1 and 2). Cells' population consists of objects of various shapes and size dispersed or closely located one to another. In particular, flattened cells show various characteristics of the cells' regions such as the cell's body itself, the cell pseudopodia region and the cell nucleus region. All these regions' characteristics vary what causes the situation in which the segmentation criteria should be locally adjusted,
- cells' population is also non-homogenous in the terms of intensity of light emission because of the difference in amount of fluorescent protein and because of the lighting decrease in time. Moreover, the distribution of fluorescent protein is not homogenous within the cell body: it is strong inside of the central region, moderate in the peripheral regions and weak in the pods developed by the cell to communicate or to move. All these features can be observed in Figs. 1 and 2, the texture is the most remarkable feature which allows us to distinguish the cell's area from the background. The background area is relatively homogeneous because the background grey level variation is caused only by the noise. The grey level variations within the cell's body region are higher than in the background because they are magnified by light absorption, reflection and amplification within the cell structures,
- thin pods are slightly visible through the texture because they are transparent as they are built by clean actin net without any granules inside but it can mostly be detected due to the week fluorescent signal emission,
- cells located closely one to another (with or without touching each other) are selected by the texture as one object and can be separated using fluorescent signal profile or other external information.

2. Proposed method

2.1. Method outline

The proposed approach to the segmentation of cell image consists of two principal stages: the coarse segmentation and the fine segmentation. The aim of the coarse segmentation is to find all the regions of the images where the cells are visible in the BF and/or EF images. In the fine segmentation stage, the precise cell boundaries are extracted.

Two complementary tracks of the coarse segmentation are proposed. The first one makes use of textural information in the BF images to produce the coarse segmentation result [31]. The second one processes the fluorescent images to achieve the same goal based on intensity of the fluorescent light emission using thresholding.

The choice of the coarse segmentation track depends on position, shape and texture of the particular cells. The combination of both results can, however, be done using the sequence of morphological image processing operators [32–35,37].

By combining both results, the final result of a coarse segmentation is obtained. This result, along with the bright field input image, is used to perform the fine segmentation. This step is performed by means of the watershed transform preceded by the gradient extraction and modification based on the combined result of the coarse segmentation. The whole process results in the precise outline (boundaries) of cells. All steps are described below. They will be illustrated on the images shown in Fig. 2.

2.2. Coarse segmentation

2.2.1. Texture-based approach

Bright-field images are characterized by a relatively low contrast. In order to improve it, the classic contrast stretching method is used

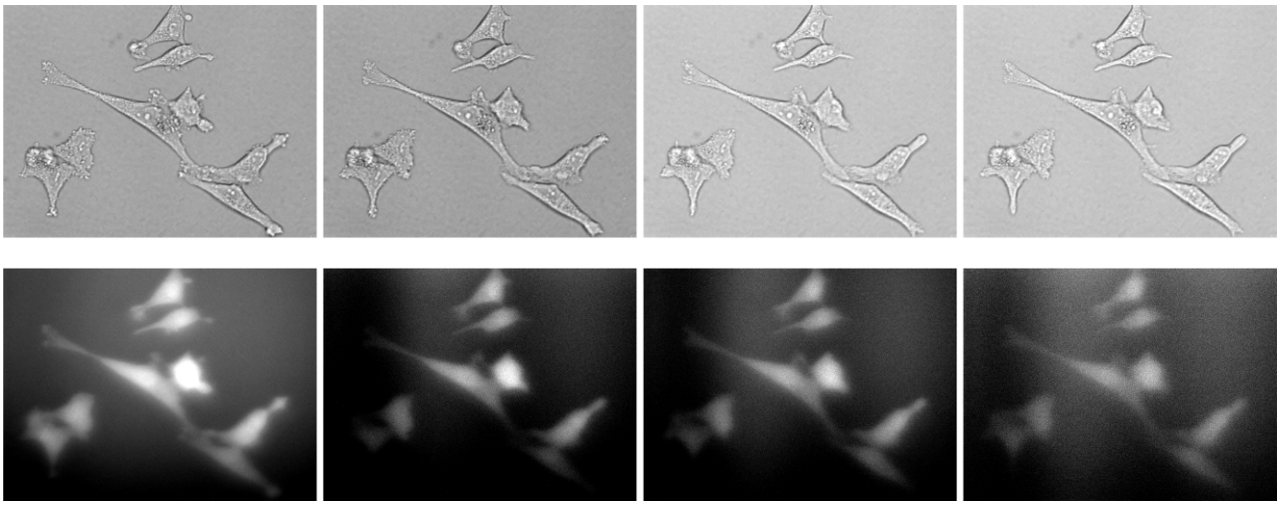

Fig. 1. Image subsequence of every third pair of images (upper row BF, bottom row EF) from image sequence captured with the time increments Δt = 6 minutes which shows nine flattened cells.

$$f_1(p) = \begin{cases} 0 & if \quad f_{BF}(p) < t_{low}, \\ \dfrac{f_{BF}(p) - t_{low}}{t_{high} - t_{low}} & if \quad t_{high} \geq f_{BF}(p) \geq t_{low}, \\ v_{\max} & if \quad f_{BF}(p) > t_{high}, \end{cases} \quad (1)$$

where f_{BF} and f_1 stands for the initial (bright-field) and the stretched image, respectively, $v_{\max}$ is the maximum possible pixel intensity. The parameters t_{low} and t_{high} stand for the lower and the higher thresholds computed by using the following equations

$$t_{low} = \min\left\{t: \sum_{i=0}^{t} h_i(f_{BF}) > \alpha\right\};$$
$$t_{high} = \max\left\{t: \sum_{i=t}^{v_{\max}} h_i(f_{BF}) > \alpha\right\}, \quad (2)$$

where $h_i(f)$ stand for the number of pixels of the intensity i in the image f (i-th bin of the histogram). The parameter α represents the cut level which refers to the number of irrelevant pixels of extreme intensities to be cut.

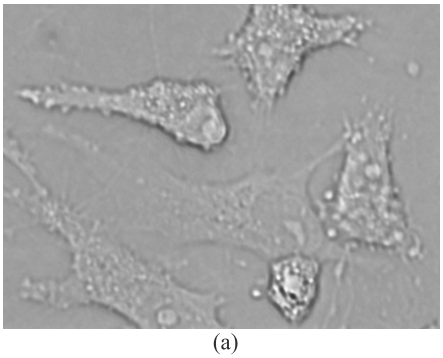

(a)

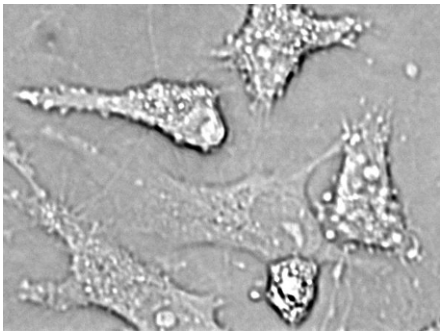

(b)

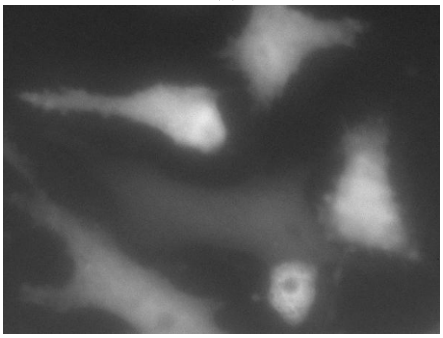

(c)

Fig. 2. Captured images: (a) bright-field image as it was acquired, (b) bright-field image after contrast increscent according to Eqs. (1) and (2) with the cut level of $\alpha = 300$, (c) fluorescent image.

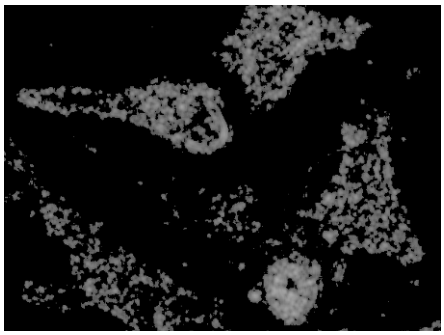

(a)

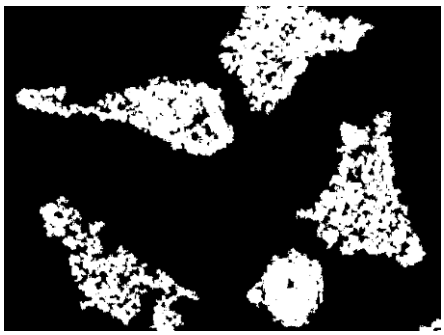

(b)

Fig. 3. Stages of processing in the texture-based approach: (a) mean absolute deviation and (b) thresholding.

The image regions referring to cells differ from the image background in terms of intensity of the texture. The background is characterized by almost homogeneous grey levels, while the cell-regions are strongly textured. Due to the latter, the simple thresholding of the input image would not produce any valuable results of the segmentation and the texture based approach must be applied.

In order to measure texturing around every pixel, the local mean absolute deviation is used. The formula of local mean absolute deviation filter can be expressed in terms of an averaging filter used twice. Such filter is used in the proposed method in the following manner

$$f_{MAD} = \left|f_1 - f_1 * \mathbf{m}\right| * \mathbf{m}, \quad (3)$$

where "*" stands for the averaging filter operator, $\boldsymbol{m}$ is the filter mask of the size $n \times n$.

The result of filtering reflects the presence of textured areas referring to the cells. On the other hand it contains a lot of noise. In order to remove this noise, the morphological opening by reconstruction is used. This filter consists of erosion followed by the morphological reconstruction and it removes small object lighter than the background without modifying the shape of the remaining image parts. It is defined as

$$f_2 = \tilde{\gamma}_B(f_{MAD}) = R^{\delta}_{f_{MAD}}[\varepsilon_B(f_{MAD})], \quad (4)$$

where $\varepsilon_B(f)$ stands for the erosion of image f with the structuring element B and R^{δ}_f is the morphological reconstruc-

tion by dilation with a mask equal to the image f and the marker image represented by its argument.

Image filtered using the morphological opening by the reconstruction is a grey-tone one, where the image parts referring to the cell regions are characterized by a higher, relatively uniform intensity, while the background consists of pixels of a low intensity value. In order to get the final result of the textural coarse segmentation, this image is thresholded at a certain intensity level. The threshold is computed as the maximum intensity of a pixel in the thresholded image multiplied by the ratio t. The final binary image f_T is thus produced as

$$f_T = f_2 > t \cdot \max_p \{f_2(p)\}. \tag{5}$$

Alternatively, the threshold can also be obtained automatically using the Otsu method [38]. The image f_T reflects well the presence of cells in the particular regions of the initial image, but the boundaries of cells are not precise enough (which is due to the linear approach in mean absolute deviation filter resulting in some blurring). The results of such filtering and the final thresholding are presented in Figs. 3(a) and 3(b), respectively. The image f_T is the final result of the method of the coarse segmentation based on texture.

2.2.2. Fluorescence image-based approach

The coarse segmentation in the second method is performed at the EF image. The EF images are characterized by a relatively high level of noise and by non-uniform intensity of the emission light distribution across the cell. In order to remove the noise, a morphological opening filter (erosion followed by dilation) is applied

$$f_3 = \gamma_B(f_{EF}) = \delta_B[\varepsilon_{B^T}(f_{EF})], \tag{6}$$

where f_{EF} stands for the input EF image, ε_B and δ_{B^T}, are for the erosion using the structuring element B and dilation with the transposed structuring element B^T of its argument (in case of symmetric structuring elements which are used in current study, $B = B^T$).

The filtered image is then binarized by thresholding, similarly to the case of the textural method relative to the maximum pixel value

$$f_E = f_3 > t \cdot \max_p \{f_3(p)\}. \tag{7}$$

As a result the binary image f_E representing the cell body area is obtained. Also in this case, the automatic threshold computation using the Otsu method can be used alternatively. The results of the morphological filtering and the final thresholding are presented in Figs. 4(a) and 4(b), respectively. The image f_E is the final result of the coarse segmentation based on fluorescence.

2.3. Marker extraction

Two results of the coarse segmentation are next combined in order to produce a unified result of the coarse segmentation, denoted as f_C. The way the image f_C is created depends on the way the particular cell appears on the microscopic image. One can distinguish several typical cases which depend on the types of cells and their relations between both coarse segmentation results. All these cases, for the sake of clarity, will be discussed using the artificial image – results of the coarse segmentation of hypothetical cells. Nevertheless, the conclusions were drawn based on the observations of cells on the real images.

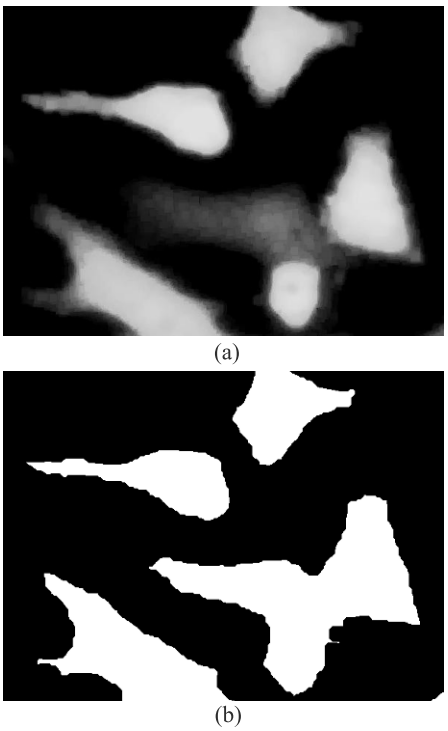

Fig. 4. Stages of fluorescence-based approach: (a) mean absolute deviation and (b) result of thresholding.

Figures 5(a) and 5(b) present images f_T and f_E, respectively. These images consist of several markers. Let us assume that every marker reflects a single cell on the hypothetical input image. Taking into account their mutual position, the following cases can be formulated:

- The cell marker is visible only on one coarse segmentation result, either f_T or f_E [case B, C, and D – see Fig. 5(c)]. In this case, this marker, no matter from which image, should be kept.
- The cell marker on f_E is entirely included in cell marker on f_T (case A). In such a case, the larger marker should be further considered (i.e., the one visible on f_T).
- The cell marker on f_E is shifted comparing to cell marker on f_T (case E). According to our observations, in this case the marker f_T from the texture be taken into account, while the other one should be rejected.
- The cell marker on f_E is considerably larger than the one on f_T (case F). In such a case, the larger region (from f_E) should be kept.

The first three of the above cases are caused by variations of the fluorescent signal strength, while the last one is caused by the undetectable texture in some parts of the flattened cells.

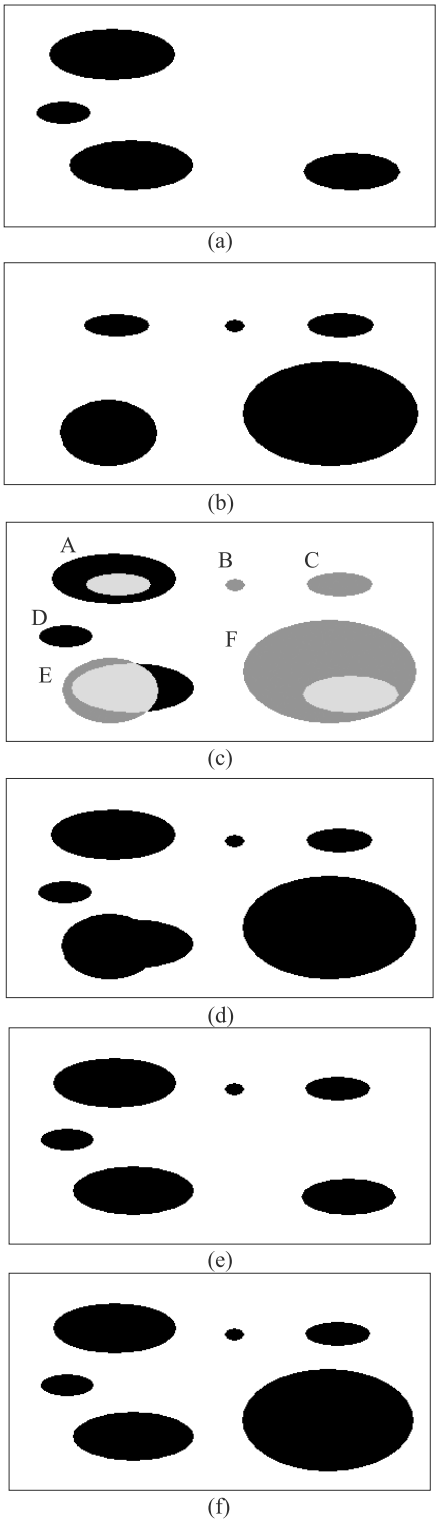

Fig. 5. Marker combining: (a) result of texture-based approach, (b) result of fluorescence-based approach, (c) sum, (d) combination type 1 and (e) combination type 2.

The strength of the fluorescent signal depends on the amount and distribution of the fluorescent protein. A compact and rounded cell produces stronger light than a large flattened one even if the total amount of fluorescent protein is the same. The consequence of natural burnout is a weakening of the fluorescent signal in time. When the light is not detectable as being below the threshold (case 1) or is detected only in some location inside the cell (case 2), the textural marker should not be modified by the florescent marker in such cases. The case 3 concerns small and compact cell with the strong fluorescent signal. This type of the cell disperses light around. It is visible as a weak, but sometimes still detectable, light rim in the nearest neighbourhood of the cell. This rim is located in the background without any detectable texture and it should be reduced from f_C. But in some cases f_E should be added to f_T. It is the case when a clean actin net in the cells' pods does not produce texture but a weak fluorescent signal is detectable. In order to distinguish both cases, the shape and size of the region is examined. So, the area shaped differently than typical rim and located just near the flattened cell is included to f_C.

Considering the above remarks, the method for combining the images f_T and f_E was developed. It will be described in the following three steps. In order to fulfil the requirements from the above points 1 and 2, a simple union of both images can be computed

$$f_C = f_T \cup f_E. \tag{8}$$

The result of such approach is shown in Fig. 5(d). Unfortunately, taking the simple union does not allow to extract properly the marker of cells according to requirements 3 and 4. In order to fulfil requirement 3, the union of f_T and only those objects from f_E that have an empty intersection of the objects on f_T should be computed. This operation (combination type 1) is performed using the morphological reconstruction by dilation

$$f_C = f_T \cup [f_E - R^{\delta}_{F_E}(f_T \cap f_E)]. \tag{9}$$

The result of such approach, shown in Fig. 5(d), fulfils the third requirement but still does not fulfil the fourth one. In order to do it, another component should be added to the union. This component represents big fragments of $f_E - f_T$ obtained by using the opening by a reconstruction filter

$$\begin{aligned} f_C = f_T &\cup [f_E - R^{\delta}_{F_E}(f_T \cap f_E)] \\ &\cup R^{\delta}_{F_E - F_T}[\varepsilon_B(f_E - f_T)]. \end{aligned} \tag{10}$$

The final result is presented in Fig. 5(f). The structuring element B used by erosion is the only parameter of this part of the algorithm. It determines the size of the added elements. This approach, as it can be easily shown, fulfils all four requirements and thanks to that the fact fits in the best way to the images considered in the current study.

2.4. Fine segmentation

The final result of the coarse segmentation is used to produce markers for the watershed segmentation which refines the outline of cells, so that their precise borders are detected. The fine segmentation stage consists of three principal

steps: gradient computation, minima imposition and watershed transform. All these steps are described in the following subsections.

2.4.1. Gradient computation

Since the watershed should be computed on a gradient image, the gradient of an input image must be obtained first. There exists, however, an important property of the input BF images that requires a special type of gradient to be used. This property refers to the "halo" effect which is visible around the cells. This effect is visible as a non-continuous, dark up-to-5-pixel thick boundary which separates the uniform background and the textured cell body. Commonly used gradient detectors (e.g., linear: Prewitt, Sobel) detect changes of intensity within the closest pixel neighbourhood. Such a gradient applied in our case would result in double gradient peaks describing the cell boundary: first peak referring to the boundary between the halo and the background, and the second one between the halo and the cell body. This would not be a desirable effect because what is needed is a single peak describing the boundary on the top of which the watershed line could be constructed. A solution to this problem requires the application of a morphological thick gradient. Both versions of such a gradient can be considered by erosion and by dilation. They are defined respectively as follow

$$f_G = f_{BF} - \varepsilon_B(f_{BF}), \tag{11}$$

$$f_G = \delta_B(f_{BF}) - f_{BF}, \tag{12}$$

where B stands for the structuring element which in the case of thick gradient contains wider pixel neighbourhood (not only the closest neighbours as in the classic morphological gradient).

The structuring element B used in the thick gradient should be chosen as the smallest one but such that the image f_G does not contain double cell boundaries.

2.4.2. Minima imposition

Minima imposition is an operation which modifies gradient in order to force the presence of image regional minima (crucial for correct result of the watershed) in given image regions and to remove unwanted existing minima. This operation is based on the morphological reconstruction and flattens all the regional minima which are not marked by a supplementary binary image – a marker image. It produces new minima in all regions which are marked by the pixels of marker image of value 1. It is a typical supplement of the watershed transformation, where the marker image is created separately in such a way that each marker points either at particular object present on the input image or points at the background. Thus, two kind of markers are possible: inner, which indicates objects (in our case: cells) and outer that points at the background area. Minima imposition with such markers guarantees that the watershed line will be located inside the area between the inner and outer markers.

(a)

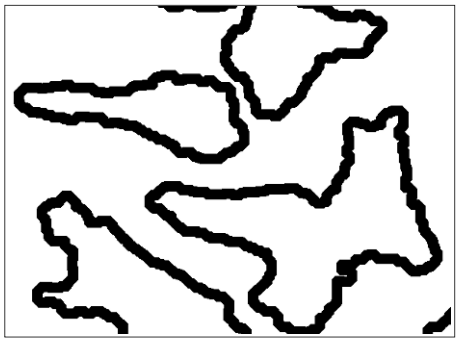

(b)

Fig. 6. Markers for the minima imposition: (a) sum of coarse segmentation results and (b) final marker.

The markers are created in the current study based on the final result of the coarse segmentation. At first, this image is processed using two consecutive morphological operators. First of them – a closing filter consisting of dilation followed by erosion, merges disconnected particles of the mask. The second one – a hole-filling fills all the holes inside these particles

$$f_4 = FH[\varphi_B(f_C)] = FH\{\varepsilon_B[\delta_{B^T}(f_C)]\}, \tag{13}$$

where FH stands for the fill-hole operator. In order to produce the inner markers, this result of both operators described above is eroded. Erosion is necessary to leave some free space inside which the watershed line could be produced. Next, the result of erosion is treated through the opening by a reconstruction operator which removes small pixel groups that could disturb further processing and which does not destroy the remainder of the image

$$f_{inner} = \tilde{\gamma}_{B1}[\varepsilon_{B2}(f_4)]. \tag{14}$$

The inner markers are thus located inside the cell bodies. Next, the inner markers are supplemented next by the outer markers. The goal for producing the outer markers is to get regions which are located outside the cells within the background area. This region is produced by next erosion, but this time, of the negative image

$$f_{outer} = \varepsilon_B(\bar{f}_{inner}), \tag{15}$$

where stands for the negative of inner markers.

Finally, the union of both markers is computed

$$f_{\text{markers}} = f_{inner} \cup f_{outer}. \tag{16}$$

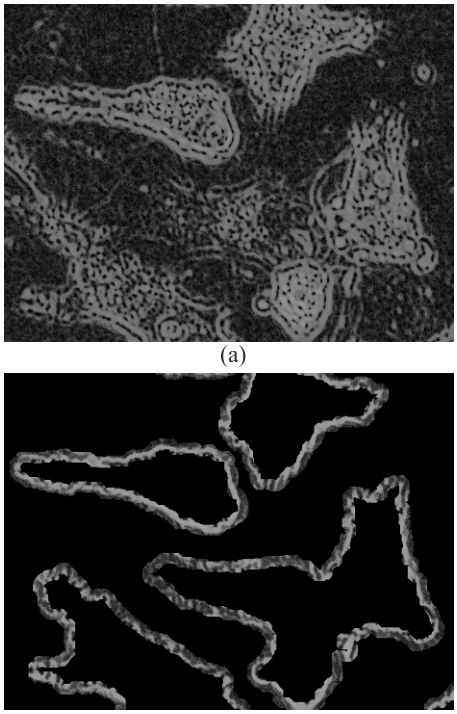

(a) (b)

Fig. 7. Minima imposition: (a) thick gradient and (b) gradient with imposed minima.

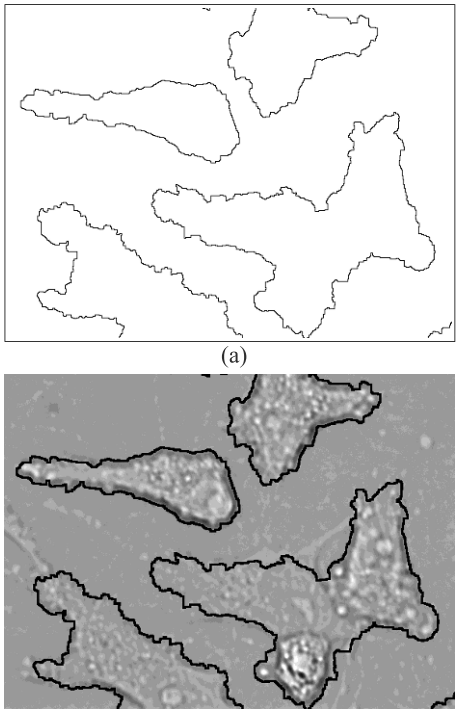

(a) (b)

Fig. 8. Result of watershed segmentation: (a) binary outline of cells and (b) outline superimposed on bright-field input image.

The union of markers covers the image regions where the boundaries of cells are not located. Its negative forms a belt around each cell where a fine boundary will be searched for. The marker extraction results are shown in Fig. 6(a) – the combined result of the coarse segmentation and in Fig. 6(b) – the markers. The union of markers is so used to impose minima on the gradient image. The gradient image and the minima imposition results are presented in Figs. 7(a) and 7(b), respectively.

2.4.3. Watershed transform

The goal of the morphological watershed segmentation is to improve the result of the coarse segmentation in order to get the fine cell boundaries. The morphological watershed segmentation aims at producing a binary image that consists of lines precisely following the boundary of an object present on the input grey-tone image.

A typical way of applying the morphological watersheds to image segmentation makes use of a gradient image as an input one for the watershed computation. In such a way, the watershed line goes on all the crest lines of the gradient. Also such a line goes around all the regional minima of the gradient image. Due to the latter, the quality of the segmentation depends strongly on a number of regional minima of the gradient image. Too many regional minima result in the over-segmentation. In order to get the proper segmentation, a number of the minima must be reduced in such a way that every single minimum refers to one object present on the original image. All unwanted minima should be thus removed before the watershed segmentation starts to run. This step was described in the previous section. The thick gradient image with the imposed minima derived from the coarse segmentation result makes thus the input for the watershed transform. Its output is the final result of the fine segmentation and consists of a line precisely following the cells' boundaries. The final result of the watershed segmentation and the same image superimposed on the input bright-field image are presented in Figs. 8(a) and 8(b), respectively.

3. Results

3.1. Images under study

3.1.1. Experimental material

The neural stem cells' line derived from the human umbilical cord blood (HUCB-NSC), established and transfected *gfp* in the NeuroRepair Dep. Lab., the Mossakowski Medical Research Centre PAS [39], were used in the experiments. The stem cells were seeded onto plastic culture dishes with a density of 105 cell/ml in standard conditions (37 °C, 5% CO_2 and 95% humidity) for 24 h (for details see Refs. 40 and 41). Then, the images' alternating sequences with the BF and EF images were acquired using the Cells Behaviour Monitoring System (CBMS; IBBE PAS), with a CoolSNAP-Pro cf camera mounted on an Olympus IX70 inverted microscope (objective x40, 0.60 NA, WD 2.6) with controllers of shatters' position.

Twelve sequences of the images were captured with time increments equal to 1–30 minutes and with a hardware

delay t_{delay} = 25 ±1 seconds. All images were captured as monochrome 1392×1040 pixels, 12 bits deep grey scale images showing the culture dishes area of 220×165 μm and documented the cells' behaviour totally in 8 h and 34 min and totally in nearly 200 pairs of images.

Every third image out of one image sequence captured with the time increment Δt = 6 minutes, was shown in Fig. 1.

3.1.2. Artificial images

Twenty pairs of the images with 50 simplified cells in all of them were constructed. Twelve of the cells were located as a single cell in the image while the rest were located as the cells' clusters with some cells separated by the background. The size of the artificial images varied: in the case of the images with a single cell in it – the size was adjusted to the centrally placed object visible with the background margin width of 20 pixels in each direction (from 180×180 up to 550×550 pixels), while in the case of the images with the clusters in it – the size was similar to experimental samples (1392×1040). Although the number of grey-tones in the artificial images were decreased (8-bit images with only 12 chosen grey-tones homogeneously distributed across the greyscale), the cells in these images were similar to those in the images from the experimental samples.

The cells in the artificial samples were constructed according to the methodology described in Ref. 42, which did not produce any shape and size simulation, but used shapes observed in the experimental samples as the simple cell template. Then, the BF image texture and the EF image intensity were simulated, based on the random Markov chains and the flattening coefficient (see samples of the artificial cells' images in Fig. 9 A – compact and rounded, B – transitional and C-large and flattened).

The cells' volume and fluorescent sustention were assumed to be constant for each cell, while the degree of cell flattening was calculated on the basis of the area covered by the cell on the template image. It was assumed that the flattening coefficient equalled 1 for the smallest, rounded and compact cells and with the shape of their projection area almost circular (cell A in Fig. 9), whilst the coefficient equalled 10 for the largest shaped irregularly cells (cell C in Fig. 9). All values of the flattening coefficient between 4 and 7 were produced by the transitional cells with various degrees of the podia development (cell B in Fig. 9). For example, the flattened cell in the BF image (cell C in Fig. 9) showed the broad and several finger shaped thin lamellas, the nucleus with nucleotides inside and the complicated texture of endoplasmatic reticulum around, typical for this type of cells. The flattened cells are the large simplified shape cells with a bright spot in the EF image, brightest in the centre and faded with an increasing distance from the centre.

Finally the suitable characteristic noise is added to both types of images.

The result of the artificial image segmentation imposed on the cell template and the BF image was presented in Fig. 9, in the right and in the middle right sectors.

The artificial image of various types of cells was constructed to evaluate the segmentation error and to compare the results of segmentation with the cell template treated as "the gold standard". The results of the error estimation were presented in the next section.

3.2. Method validation

This method required several parameters which should be chosen according to the resolution of the image. Table 1 shows the values of all parameters used in validation of the method for the images captured during the experiments and for the artificial cells' images.

As it is shown in Table 1 the thresholds and the size of an area left as the pods region sometimes need to be adjusted,

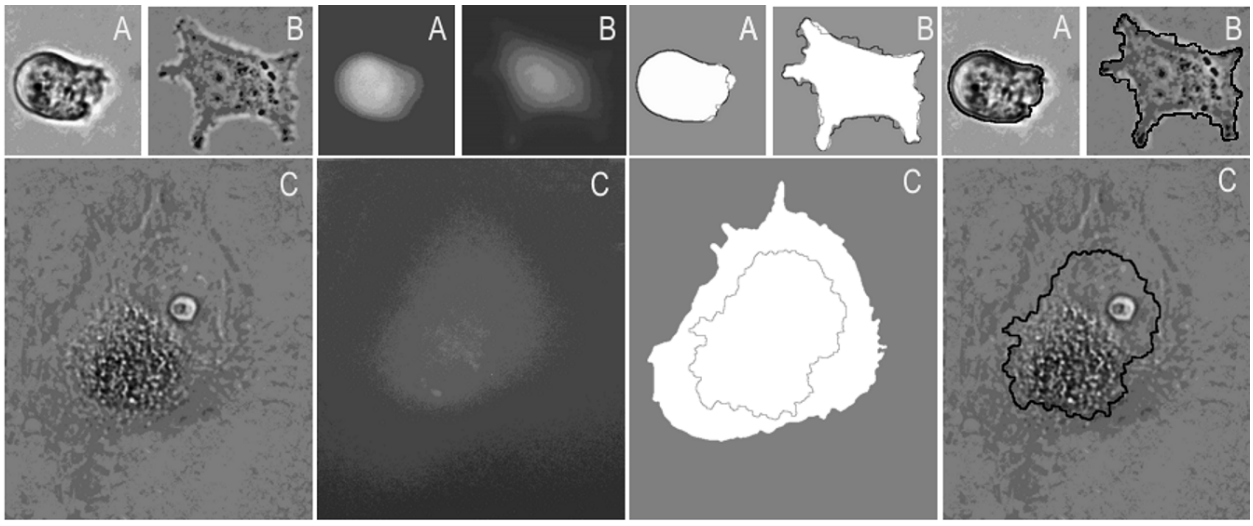

Fig. 9. The artificial images of cell: A – compact and rounded cell, B – transitional cell, C – flattened cell; image sectors: the left – artificial BF image, the middle left – artificial EF image, the middle right – results of the segmentation imposed on the template image and the right – results of the segmentation imposed on the BF image.

Table 1. Values of parameters used in proposed method of segmentation.

Eq.	Parameters	Remarks	Eq.	Parameters	Remarks
2	$\alpha = 300$		9	B – ball of radius 10	Sometimes even up to 15
3	$n = 5$	Size of mask $\boldsymbol{m}$	11, 12	B – ball of radius 5	Eq. (11) used
4	B – ball of radius 7		13	B – ball of radius 7	
5	t – Otsu method or chosen threshold	In most cases Otsu, but sometimes for natural 0.3–0.6 of maximal intensity	14	B_1 – ball of radius 5	
6	B – ball of radius 9		14	B_2 – ball of radius 2	
7	t – Otsu method or chosen threshold	Mostly 0.1–0.3 of maximal intensity and sometimes Otsu	15	B – ball of radius 5	

while the rest of parameters have been fixed as dependent on the microscope magnification only. The texture threshold [(Eq. (5)] is mostly selected by the Otsu threshold and rarely adjusted by the interactively selected α while the fluorescence image threshold [(Eq. (7)] is more dependent on the interactively selected α. The Otsu threshold calculated for the EF images becomes efficient after the image pre-processing which reduces non-homogeneity of the light distribution by the background levelling (see Fig. 1).

The results of segmentation of two experimentally acquired sequences and of 20 artificial pairs of the images were analyzed visually and partly quantitatively. Since there was no "gold standard" for experimentally collected samples, the artificial image segmentation results were only used to assess two types of errors: object area error and object location error [43,44].

The cells' area error E was calculated with the following formula where B^r is the segmentation result and B is the "gold standard" area

$$E = \frac{[(B \bigcup B^r) - (B \bigcap B^r)]}{\overline{B}} \times 100\% . \qquad (17)$$

The error of object location E was measured on the basis of a position of the cell centre, as the centre of the lamina model of cell projection on the observation plane. This error was measured by the distance between the expected and the calculated centres with accuracy of a half of a pixel.

The segmentation error was calculated for three types of cells separately:

- rounded and compact cells – with the area less than 15000 pixels,
- large and flattened cells – with the area bigger than 55000 pixels,
- transitional cells – with the area between these two values.

The results are shown in Table 2.

Table 2. Area and location error of segmentation.

Cell type (a number of cells)	Error in area (in %)	Error in location (in pixels)
Rounded and compact (10)	6 ±4	5 ±3
Transitional (20)	17 ±12	28 ±20
Flattened and large (15)	43 ±21	133 ±71

The visual examination of the experimentally collected image sequences, in which the rejection of pods was on the accepted level, similar to the level presented in Fig. 8 (with the cluster treated as an object) shows that 73% of the objects made cells or clusters segmented according to our expectation, while the segmentation procedure rejected important parts of the cells' area and/or added some parts of the background in other cases. The visual examination also agreed with the results of the artificial images error estimation: the errors were smallest for the rounded and compact cells, the errors were acceptable for the transitional cells while the errors were big for the flattened cells with broad lamellas in which the segmentation procedure reduced external parts of a cell.

4. Conclusions

The proposed MSMA method of segmentation supports biological investigations and medical diagnoses and prognosis in case of direct observation of the cells' behaviour in time. The method localizes the cells and cell clusters in the images from the sequence of microscopic images acquired by using alternately two techniques: BF and EF. This double source of information gives synergic effects in the cell area determination which allowed to support the segmentation process even in the very difficult cases as presented in Fig. 10.

The large and flattened cells in the peripheral parts are deprived from such cells' structures which produce a texture in the BF images. It makes these parts of a cell not detectable by using the texture [(Fig. 10(a) top and left parts)], while the weak fluorescent signal is still detectable. The weak fluorescent signal characterizes not only perip- heral parts of flattened cells but also the background around small and compact cells [(Fig.10(b) right bottom part)]. To avoid the background being included in the cell's area, a special method of the marker construction has been deve- loped. This method adds to the texture based marker only these parts of the fluorescent based marker which are larger than a certain area threshold. At the same time, it rejects small thin fragments around the strongly textured area [(Fig. 10(c)].

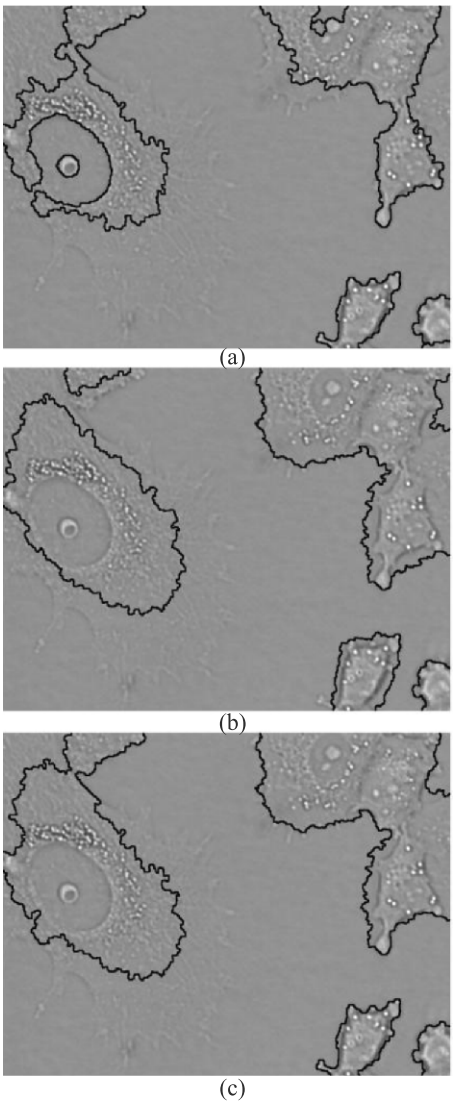

Fig. 10. Results of segmentation with the different markers constructed on the basis of: (a) only texture, (b) only fluorescence, and (c) special method of marker construction.

The proposed method is very effective and precise in case of the small and transitional cells. In the case of large and flattened cells, the detected area covered by the cell is limited to the parts textured in the BF image and to the parts which produce even weak fluorescent light in the EF image. Due to this fact, the small finger shaped protrusions are rejected from the detected cell area (see and compare bottom left part in each image in Fig. 10).

The cell centre is usually used to estimate the cells' position in the cell movement investigation. The gravity centre of the lamina model of the cell are both calculated on the segmentation results and based on the cell template calculated for the artificial images. The comparison of the position of these two gravity centres allows us to conclude that even the outline of the segmented objects is not just in the position of a template, still it remains within the acceptable range of up to ten pixels distance. The error in the area detection of the rounded and transitional cells is homogeneously distributed around the cell. The position of the cell centre is close to the position of the template cell. For the flattened cells, the distance between centres is in 50% of the examined cells bigger then for the other cell types because of inhomogeneous distribution of the undetected cell fragments. But in this case the centre of a well visible nucleus can be defined as a cells' position in investigation of the cell movement.

The proposed method can be used if the EF images have not been collected. In this case the BF image and the fully black EF image make the pairs of the images and the EF image produces the empty map of lighting object in the image plane. In such a case, the accuracy and precision of results of the segmentation:

- do not decrease for the small and compact cells,
- slightly decrease for the transitional cells,
- significantly decrease for the flattened and large cells.

This type of segmentation is suitable for investigation with counting of a number of cells in the image plane without its whole body examination and in the cells' movement estimation.

The method is semi-automatic because the operator adjusts its parameters in some cases according to the object properties and, therefore, it is much faster and the results are more reproducible than the results achieved according to any type of the manual segmentation.

The proposed segmentation method can be considered as the core of algorithms for the microscopic image sequences segmentation. In this case, the information about results of the segmentation of the previous frames can be used to segment next frame as the time increment of the cells' behaviour observation provides that the cells from one frame to the other do not change its shape and location rapidly.

Acknowledgements

This work was supported by the Ministry of Science and Higher Education of Poland (MNiSW), research project no. 3911/B/T02/2008/34 of the financial support for science in 2008–2011. We are grateful for the transfected *gfp* neural stem cells line HUCB-NS from the NeuroRepair Dpt. Lab., MRI, PAS.

References

1. L. Mirosław, A. Chorążyczewski, F. Buchholz, and R. Kittler, "Correlation-based method for automatic mitotic cell detection in phase contrast microscopy", *Adv. Soft Comp.* **1**, pp. 627–634, edited by M. Kurzyński, E. Puchała, M. Woźniak, and A. Żołnierek, Springer-Verlag, Berlin Heidelberg, 2005.
2. R.T. Proffitt, J.V. Tran, and C.P. Reynolds, "A fluorescence digital image microscopy system for quantifying relative cell numbers in tissue culture plates", *Cytometry* **24**, 204–213 (1996).
3. D. Lewińska, J. Bukowski, M. Kożuchowski, A. Kinasiewicz, and A. Weryński, "Electrostatic microencapsulation of living cells", *Biocybern. Biomed. Eng.* **28**, 69–84 (2008).

4. J. Boezeman, R. Raymakers, G. Vierwinden, and P. Linssen, "Automatic analysis of growth onset, growth rate and colony size of individual bone marrow progenitors", *Cytometry* **28**, 305–310 (1997).
5. A. Korzyńska, M. Jurga, K. Domańska-Janik, W. Strojny, and D. Włoskowicz, "Analysis of stem cell clonal growth", *Adv. Soft Comp.*, **1**, pp. 577–584, edited by M. Kurzyński, E. Puchała, M. Woźniak, and A. Żołnierek, Springer-Verlag, Berlin Heidelberg, 2005.
6. A. Korzyńska and M. Zychowicz "A method of estimation of the Cell Doubling time on Basis of the Cell culture Monitoring Data", *Biocybern. Biomed. Eng.* **28**, 75–82 (2008).
7. K. Jiang, Q.M. Liao, and S.Y. Dai, "A novel white blood cell segmentation scheme using scale-space altering and watershed clustering", *Proc. Int. C. Machine Learning and Cybernetics* **5**, 2820–2825 (2003).
8. Q. Liao and Y. Deng, "An accurate segmentation method for white blood cell images", *Proc. Int. Symp. on Biomedical Imaging*, 245–248 (2002).
9. B. Nilsson and A. Heyden, "Model-based segmentation of leukocyte clusters", *Proc. Int. C. Patt. Recog.* **1**, 727–730 (2002).
10. G. Ongun, U. Halici, K. Leblebicioglu, V. Atalay, M. Beksac, and S. Beksak, "An automated differential blood count system", *P. Ann. Int. IEEE EMBS* **3**, 2583–2586 (2001).
11. A. Hoppe, A. Korzyńska, and D.Wertheim "A computer system for the analysis of neutrophil movement", *Med. Biol. Eng. Comput.* **37**, 1000–1001 (1999).
12. P. Bartels, R. Montironi, V. Duval da Silva, P. Hamilton, D. Thompson, L. Vaught, and H.G. Bartels, "Tissue architecture analysis in prostate cancer and its precursors: an innovative approach to computerized histometry", *Eur. Urol.* **35**, 484–491 (1999).
13. T. Markiewicz, P. Wiśniewski, S. Osowski, J. Patera, W. Kozłowski, and R. Koktysz, "Comparative analysis of methods for accurate recognition of cells through nuclei staining of KI-67 in neuroblastoma and estrogen/progesteronestatus staining in breast cancer", *Anal. Quant. Cytol. Histol.* **31**, 49–62 (2009).
14. N. Zama and H. Katow, "A method of quantitative analysis of cell migration using a computerized time-lapse video-microscopy", *Zool. Sci.* **5**, 53–60 (1988).
15. A. Korzynska, W. Strojny, A. Hoppe, D. Wertheim, and P. Hoser, "Segmentation of microscope images of living cells", *Pattern. Anal. Appl.* **10**, 301–319 (2007).
16. A. Boucher, A. Doisy, X. Ronot, and C. Garbay, "Cell migration analysis after *in vitro* wounding injury with a multi agent approach", *Artif. Intell. Rev.* **12**, 137–162 (1998).
17. L. Witkowski, "A computer system for cells motility evaluation", *Machine Graphics and Vision* **17**, 167–186 (2008).
18. M. Iwanowski and A. Korzyńska, "Segmentation of moving cells in bright-field and epi-fluorescent microscopic image sequences", in *Lect. Notes Comput. Sc.* **6374**, pp. 401–410, edited by L. Bolc, R. Tadeusiewicz, L.J. Chmielewski, and K. Wojciechowski, Springer-Verlag, Berlin Heidelberg, 2010.
19. D.L. Pham, C. Xu, and J.L. Prince, "A survey of current methods in medical image segmentation", *Annu. Rev. Biomed. Eng.* **2**, 315–338 (2000).
20. D. Comaniciu and P. Meer, "Cell image segmentation for diagnostic pathology", in *Advanced Algorithmic Approaches to Medical Image Segmentation: State-of-the-Art Application in Cardiology*, *Neurology, Mammography and Pathology*, pp. 541–558, edited by J.S. Suri, S.K. Setarehdan, Springer, 2001.
21. H. Ramoser, "Leukocyte segmentation and SVM classification in blood smear images", *Machine Graphics and Vision* **17**, 187–200 (2008).
22. S. Tse, L. Bradbury, J.W.L. Wan, H. Djambazian, R. Sladek, and T. Hudson, "A combined watershed and level set method for segmentation of bright field cell images", *Proc. SPIE* **7258**, 72593G-72593G-10 (2009).
23. M. Wang, X. Zhou, F. Li, J. Huckins, R. King, and S. Wong, "Novel cell segmentation and online SVM for cell cycle phase identification in automated microscopy", *Bioinformatics* **24**, 94–101 (2008).
24. E. Alkuwari, K. Khetani, N. Dendukuri, L. Wang, and M. Auger, "Quantitative assessment of nuclear grooves in fine needle aspirates of the thyroid", *Anal. Quant. Cytol. Histol.* **31**, 161–169 (2009).
25. A. Dulewicz, D. Piętka, and P. Jaszczak, "Digital image analysis in research and diagnosis of urinary bladder cancer", in *Bladder Cancer: Etymology*, *Diagnosis and Treatments*, pp. 211-228, edited by W.E. Nilsson, Nova Science Biomedical Books, New York, 2010.
26. T. Markiewcz and S. Osowski, "Morphological operations for blood cells extraction from the image of the bone marrow smear", *Prz. Elektrotechniczn.* **84**, 24–26 (2008).
27. U. Neuman, A. Korzynska, C. Lopez, and M. Lejeun, "Segmentation of stained lymphoma tissue section images", in *Information Technology in Biomedicine* **2**, ASC **69**, pp. 101–113, edited by E. Pieta and J. Kawa, Springer-Verlag, Berlin Heidelberg, 2010.
28. T. Markiewicz, S. Osowski, J. Pater, and W. Kozlowski, "Image processing for accurate cell recognition and count on histologic slides", *Anal. Quant. Cytol. Histol.* **28**, 281–291 (2006).
29. G. Kayser, D. Radziszowski, P. Bzdyl, R. Sommer, and K. Kayser, "Theory and implementation of an electronic, automated measurement system for images obtained from immunohistochemically stained slides", *Anal. Quant. Cytol. Histol.* **28**, 27–38 (2006).
30. C. Lopez, M. Lejeune, M,T. Salvedo, P. Escriva, R. Bosh, L.E. Pons, T. Alvaro, J. Roig, X. Cugat, J. Baucells, and J. Jaen, "Automated quantification of immunohistochemical markers with different complexity", *Histochem. Cell Biol.* **129**, 379–287 (2008).
31. R.M. Haralick, K. Shanmugam, and I. Dinstein, "Textural features for image classification", *IEEE T. Syst. Man Cyb.* **6**, 610–621 (1973).
32. M. Iwanowski, *Morphological Methods in Digital Image Processing*, AOW EXIT, Warsaw, 2009. (in Polish)
33. M. Nieniewski, *Mathematical Morphology in Image Processing*, PLJ, Warsaw, 1998. (in Polish)
34. M. Iwanowski and J. Serra, "The morphological-affine object deformation", *Mathematical Morphology and its Applications to Signal and Image Processing*, pp. 81–90, Kluwer Academic Publishers, 2000.
35. J. Serra, *Image Analysis and Mathematical Morphology*, Academic Press **1**, 1983.
36. J. Serra, *Image Analysis and Mathematical Morphology*, Academic Press **2**, 1988.

37. P. Soille, *Morphological Image Analysis: Principles and Applications*, Springer-Verlag, 2004.
38. N. Otsu, "A threshold selection method from grey level histograms", *IEEE T. Syst. Man Cyb.* **9**, 62–66 (1979).
39. L. Bużańska, E.K. Machaj, B. Zabłocka, Z. Podja, and K. Domańska-Janik, "Human cord blood-derived cells attain neuronal and glial features in vitro", *J. Cell Sci.* **115**, 2131–2138 (2002).
40. M. Iwanowski and A. Korzyńska, "Detection of the area covered by neural stem cells in cultures using textural segmentation and morphological watershed", *Adv. Soft Comp.* **3**, pp. 543–557, edited by M. Kurzyński, E. Puchała, M. Woźniak, A. Żołnierek, Springer-Verlag, Berlin Heidelberg, 2009.
41. http:\www.ibib.waw.pl/grants/korzynska
42. A. Korzyńska and M. Iwanowski, "Artificial images for evaluation of segmentation results; bright field images of living cells", accepted for *LNCS*, 2012.
43. Y.J. Zhang and J.J. Gerbrands, "Objective and quantitative segmentation evaluation and comparison", *Signal Process* **39**, 43–54 (1994).
44. A. Korzyńska, M. Iwanowski, U. Neuman, E. Dobrowolska, and P. Hoser, "Comparison of the methods of microscopic image segmentation", *IFMBE Proc.* **25/**IV, pp. 425–428, Munich, 2009.

